SPACE TELESCOPE SCIENCE INSTITUTE
Operated for NASA by AURA

Instrument Science Report ACS 2011-03

Flux Calibration of the ACS CCD Cameras

III. Sensitivity Changes over Time

Ralph C. Bohlin, Jennifer Mack, and Leonardo Ubeda
June 2, 2011

Abstract

The flux calibration of HST instruments is normally specified after removal of artifacts such as a decline in charge transfer efficiency (CTE) for CCD detectors and optical throughput degradation. This ACS ISR deals with the HRC and WFC losses in sensitivity from polymerization of contaminants on the optical surfaces. Prior to the demise of the ACS CCD channels on 2007 Jan. 27, the losses are less than ∼0.003 mag/year, except for the two short wavelength HRC filters F220W and F250W. The measurements of the sensitivity loss rates using a set of observations of WD flux standards has a precision of ∼0.0008 mag/year, while the sensitivity loss rates using repeated observations of the globular cluster 47 Tuc are probably consistent within their currently lower precision.

Following the revival of ACS WFC during the Servicing Mission 4 (SM4) in 2009 May, the gain of the new electronics was set so that the measured signal in electrons s^{-1} matched the signal for the same 47 Tuc field as measured in 2002 with the F606W filter. However, a longer time baseline is required to reliably determine the post-SM4 loss rates.

1. Introduction

In order to specify a flux calibration for the ACS CCD imaging data, the photometry must be corrected for gradual losses in the charge transfer efficiency (CTE) of the CCD

detectors and in the transmission of the optics. Both the CTE and the system throughput have been decreasing since installation of ACS into HST on 2002 March 7 (Bohlin 2007, hereafter B07). The polymerization of contaminants on the optical surfaces probably causes the gradual loss of optical throughput; and bombardment of the CCD detectors by cosmic rays causes the loss of charge transfer efficiency. However, there are two events that introduce discontinuities into this loss process.

First, after the side-2 electronics were activated on 2006 July 6, the set-point temperature was reduced from -77C to -81C for the WFC CCD in order to mitigate the impact of hot pixels (Sirianni et al. 2006). The lower operating temperature caused wavelength dependent discontinuities of up to 2.4% in the sensitivities, which were implemented in the form of new QE curves that are used to determine the $photflam$ absolute flux calibration keyword in the WFC data headers. For example in 2006 July, the $photflam$ for WFC F814W changes from 6.926e-20 to 7.033e-20 $erg\ s^{-1}\ cm^{-2}\ \mathring{A}^{-1}/(electron\ s^{-1})$, a change of -0.0166 mag and specified as -0.016 mag in Mack et al. (2007). Studies of the changing sensitivity must utilize the fluxes calibrated with the proper $photflam$ or must apply the Mack et al. corrections to the measured photometry in electrons s^{-1} for observations obtained after 2006 July 6. In addition, the lowering of the set-point to -81C caused minor flat field changes of up to 0.6%, which are automatically included in the STScI ACS pipeline data products (Gilliland et al. 2006).

The second discontinuity in the gradual loss of sensitivity was caused by the the CCD Electronics Box Replacement (CEB-R) with its ASIC sidecar circuit board during SM4 in 2009 May (Grogin et al. 2010). Because CCDs are inherently analog readout devices with arbitrary data number readout units (DN) and because the exact conversion of photoelectrons to the DN readout unit of the new ASIC is not measured in the laboratory, the post-SM4 sensitivities cannot be measured with respect to the earlier sensitivities. Thus, the WFC gain value that converts photo-electrons to DN is arbitrary. The exact value of the gain of the new electronics that converts measured DN values to electrons was established by matching the F606W stellar fluxes at an average time of 2009.6 for an average of seven 47 Tuc datasets to a mean of 18 observations of the same field obtained in 2002 April–May at an average time of 2002.4. The CTE correction algorithm of Chiaberge et al. (2009, hereafter MC09) was applied to all the 47 Tuc photometry. The 2009.6 fluxes are calculated with the $photflam$ keyword values established in 2006 July for the -81C WFC operating temperature, so that the $photflam$ values currently remain unchanged since 2006 July. However, this approach does not make the relative sensitivities at 2009.6 exactly equal to the 2002.4 values for all the WFC filters. (See §2 below). One way to correct these minor inconsistencies is to treat the post-SM4 WFC like a new instrument and adjust the WFC QE curve and throughput of each filter via post-SM4 observations of the white dwarf (WD) flux standards, so that

there would be a second discontinuity of the $photflam$ values. Alternatively for dates after SM4, our normalization of filter dependent correction of §2 can account for the sensitivity discontinuity caused by the repair of the ACS electronics in SM4.

This ISR is the third (III) in a four part series that will culminate in IV with a new flux calibration for the ACS CCD detectors. ISR I (Bohlin & Anderson 2011) defines the CTE losses for observations of the bright flux standard stars with the WFC CCD, while II (Bohlin 2011) establishes the encircled energy corrections for the fiducial 1″ radius vs. infinite (5″.5) radius. The sensitivity changes found from repeated observations of the flux standards are compared here with the results from repeated observations of the 47 Tuc field.

2. Analysis of the Standard Star Data

Because of the electronics change in 2009 May that required the establishment of new gain values, the time periods before and after the ACS failure on 2007 Jan 27 must be analyzed separately. To measure the post-2009 trends, a baseline of several observations of the standards is required over a few years. In the meanwhile, a constant sensitivity at the mean level of the post-2009 observations is adopted; and this ISR concentrates on the determination of the sensitivity loss rates prior to the 2007 ACS failure. The reference position for the flux calibration presented here is at the center of the HRC CCD and the center of the standard WFC1-1K subarray at pixel (3583,1535) on chip-1. The maximum allowed offset from the reference position is 6″.5 for HRC and 8″.4 for WFC. For the flux of sources remote from these reference positions, uncertainties in the flat field correction must be included with the uncertainties enumerated herein.

Photometry for the three WD primary standards is extracted for apertures of 0.15, 0.35, 0.65, and 1.0 arcsec, which corresponds to 3, 7, 13, and 20 pixels for WFC and double those radii in pixels for HRC. The three stars are on a common scale defined by the observed countrate C divided by the prediction from synthetic photometry P, as described in detail in B07 and Bohlin et al. (2011). The stellar SEDs for these three fundamental HST standards are the pure hydrogen NLTE models from the HST CALSPEC database[1]. The change in sensitivity for each filter is fit with a straight line; and then these slopes are fit with a polynomial as a function of the filter pivot wavelengths. For example, Figure 1 shows the fits for F555W for the one arcsec radius photometry with a background annulus from 6-8″ for WFC and from 5.5-6″.5 for HRC, which is the standard reference aperture of de Marchi et al. (2004), Sirianni et al. (2005, S05), and B07. The HRC and WFC photometry are in

[1]http://www.stsci.edu/hst/observatory/cdbs/calspec.html/

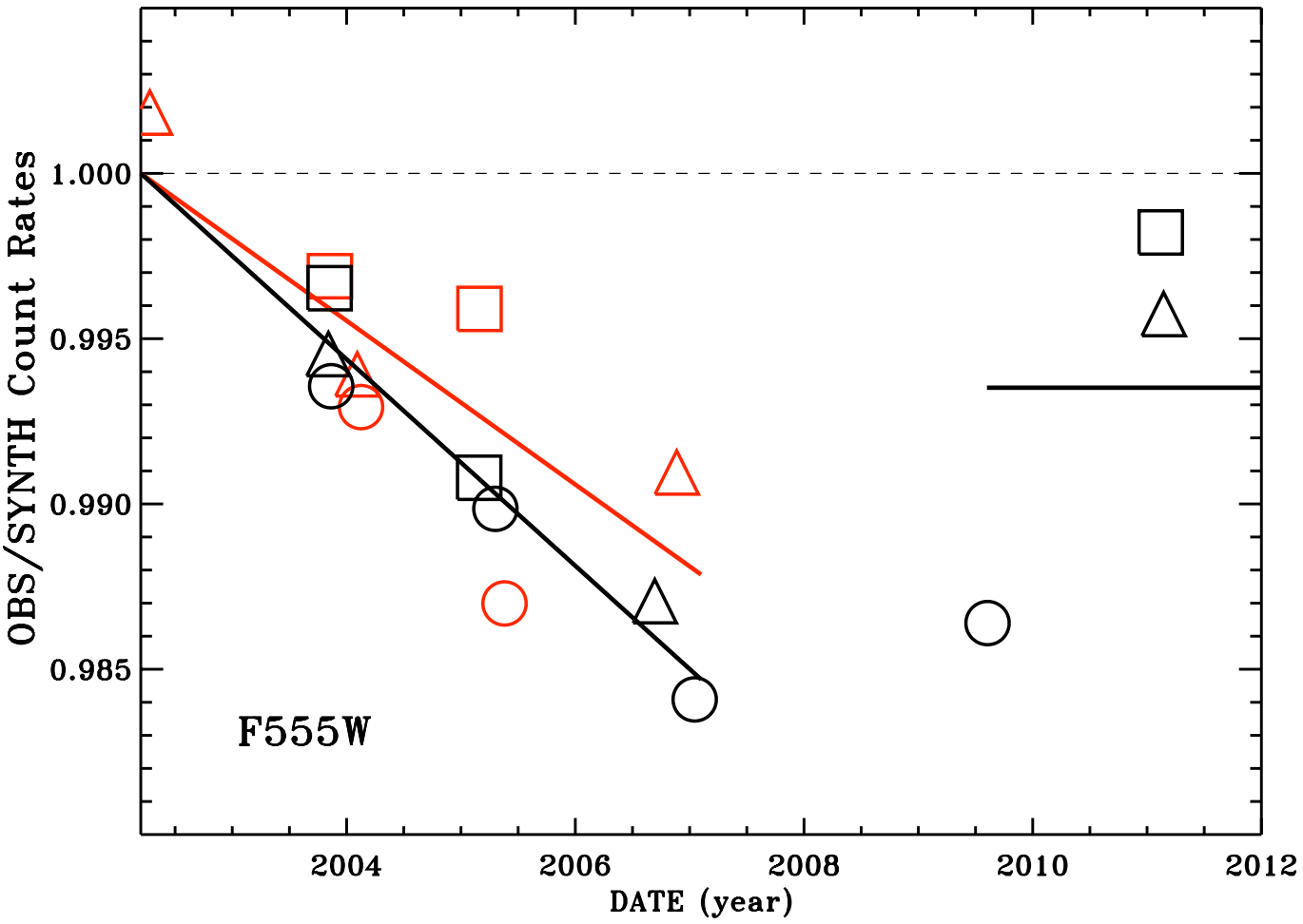

Fig. 1.— Ratio of CTE-corrected observed to predicted count rates C/P for F555W as a function of time for the one arcsec radius photometry. Symbols are: square-G191B2B, circle-GD153, and triangle-GD71. Black symbols are for WFC, and red are HRC. The 2002–2007 straight line fits and the data for each camera are normalized to the value which makes each fit equal to unity at 2002.2, i.e. the time at which the absolute flux calibration is applicable. After 2009.6, the slope is arbitrarily set to zero, pending the collection of data over a longer timeline, and the level is normalized to the average of the post-SM4 points.

red and black, respectively, along with the two separate best fits.

The parameterized correction for the CTE losses in the WFC (Bohlin & Anderson 2011) are applied before fitting the sensitivity change vs. time for the slopes of the one arcsec photometry. However, the maximum CTE correction is only 0.16% for the WFC observations of the standard GD71 at 2011.1 with F775W. Although there is no CTE correction for the HRC, those data are similarly well exposed; and any CTE correction for HRC is expected to be as negligible as the WFC CTE corrections.

For the one arcsec photometry, Figure 2 shows the slope of the loss rates for each filter and a fourth-order polynomial fit for both cameras as a function of the pivot wavelength. The narrow band data is omitted in the fitting procedure, as justified by B07. The WFC and HRC data could be fit independently with separate fits that differ the most around 4500Å because of the two high WFC points for F435W and F475W. However, the differences are less than the uncertainties of the fits; thus for simplicity, the HRC and WFC slopes are fit together. The 1σ error bars of most of the points, including both the WFC F435W and F475W, overlap the fourth-order fit. The rms scatter of 0.07%/year of the one arcsec radius photometry about the fit is the adopted uncertainty shown as dashed lines in Figure 2. In the case that degradation of the exposed OTA mirrors is the primary cause of the sensitivity losses, the excellent agreement between the WFC and HRC points in Figure 2 is not surprising. In any case, separate WFC and HRC fits that differ by 0.07%/year from the joint solution imply photometric differences of only 0.3% after 4.8 years on-orbit at the time of the failure in 2007.

The loss rates for the 0.35 and 0.65 arcsec radii photometry agree with the baseline 1.0 arcsec radius of Figure 2 within the uncertainties, which are 0.12 and 0.09%/yr for .35 and 0.65 arcsec, respectively. However, the results for 0.15 arcsec (3 pixels for WFC) are much noisier due to focus variations, i.e. "breathing" caused by the day-night thermal cycling of the orbit. The loss rates for the one arcsec aperture have the smallest uncertainties and should provide the best correction for any ACS photometry after properly accounting for the encircled enery fraction. The results differ from the previous analysis of the same data by B07 by less than the 0.07%/year uncertainty of the fit to the one arcsec data in Figure 2.

The coefficients of the fourth order polynomial fit in Figure 2 are -0.03301, 2.131e-05, -5.438e-09, 5.933e-13, -2.299e-17, while the loss rates evaluated at the average pivot wavelengths appear in Table 1.

As an interim correction for estimating the sensitivities after the 2009 SM4, a constant sensitivity is assumed as a compromise between an apparent increase suggested by the three post-SM4 data points and the expectation that the loss rate should be similar to the earlier

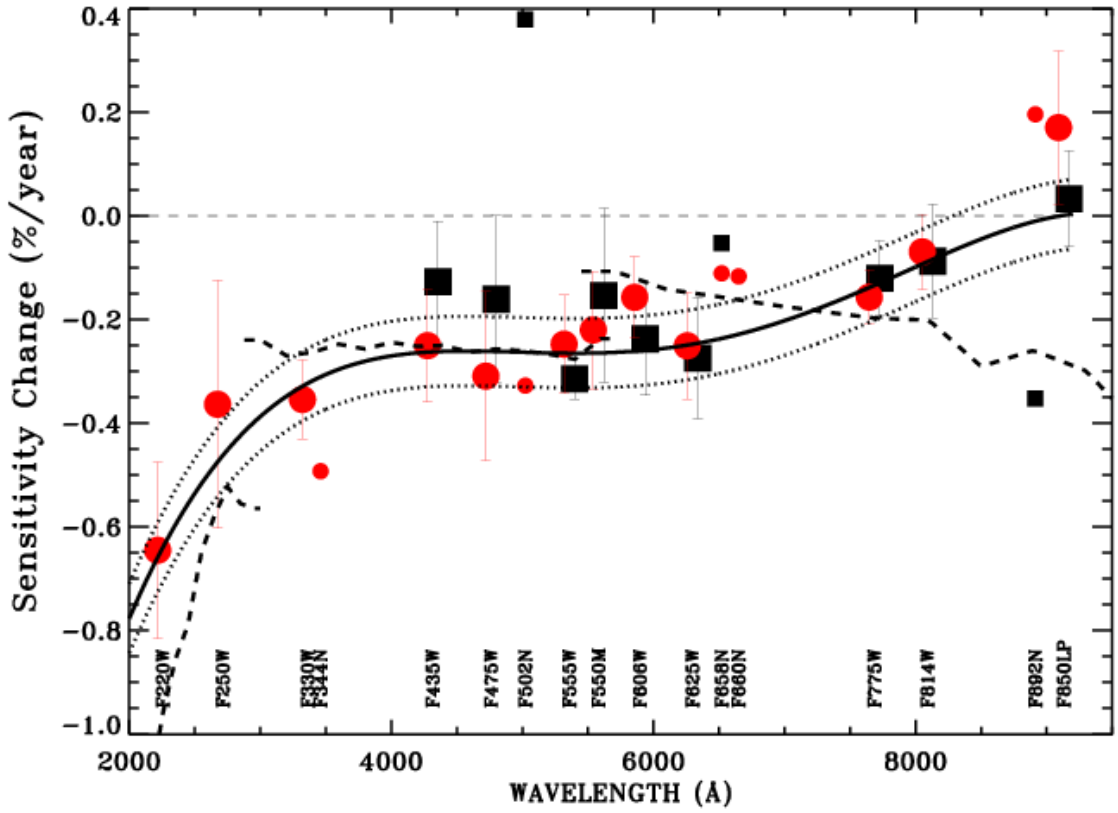

Fig. 2.— Pre-SM5 slopes in percent loss of sensitivity per year for all filters, as in the example for F555W in Figure 1. Black is for the WFC, while red represents the HRC. Large symbols are broad and medium bandpass, while small symbols are for the narrow band filters. A fourth order fit for the large symbols is shown as a function of the filter pivot wavelength with the uncertainty shown as dotted lines. Error bars on each point are the 1σ formal uncertainty in the slope of the linear fits. Most of the error bars cross the fit, and there is no systematic difference between the WFC and HRC data points. The corresponding average sensitivity losses for the three CCD grating modes of STIS (dashed lines) from (Stys, Bohlin, & Goudfrooij 2004) are similar to the ACS loss rates. Because an increase in sensitivity seems non-physical and because the data for both cameras are consistent with zero change, the fit for F850LP is set to zero.

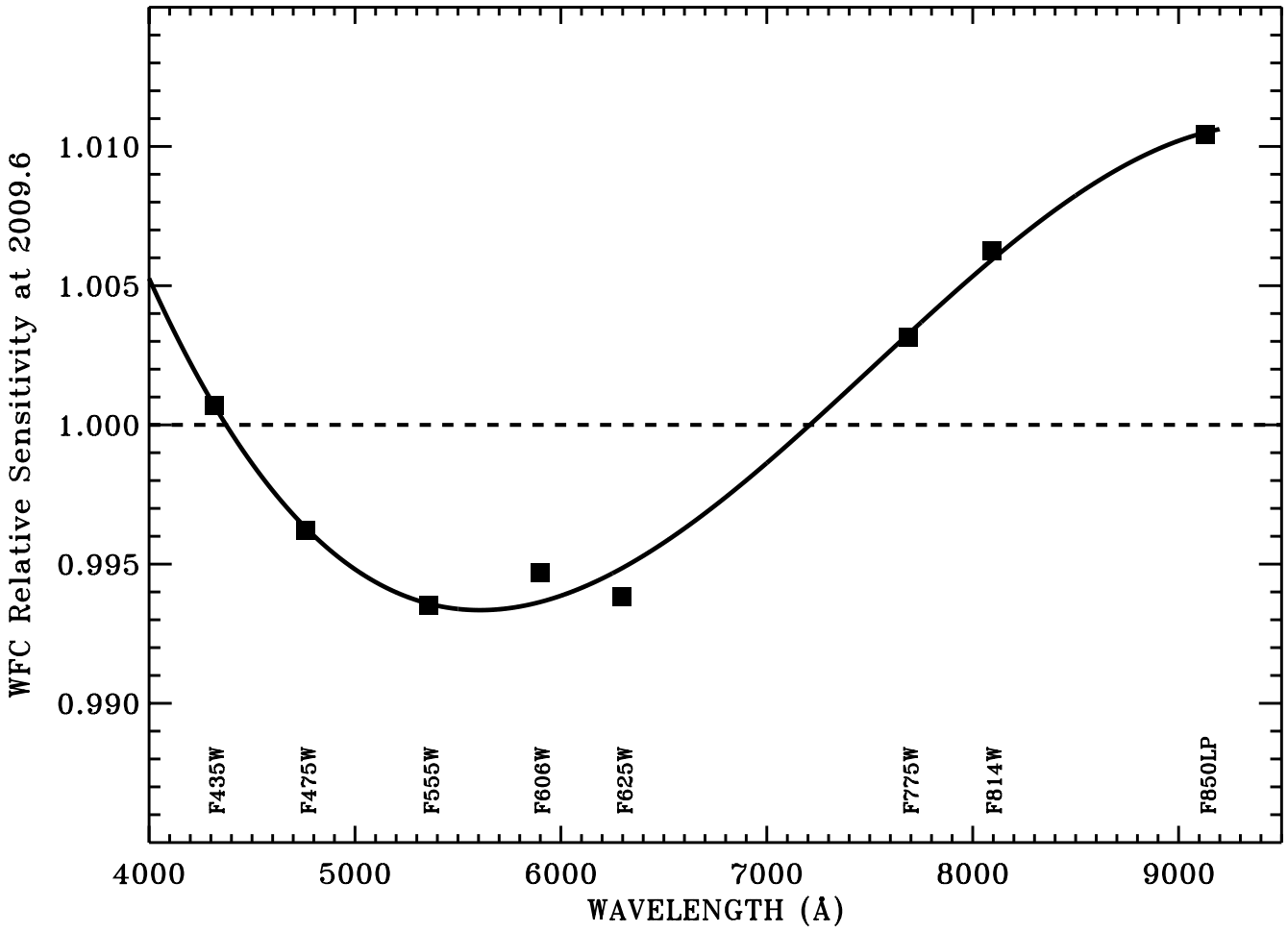

Fig. 3.— Value of the sensitivity correction at 2009.6 relative to the initial sensitivity at 2002.2 as based on the average of the three available observations with their problematically large scatter illustrated in Figure 1. The data points are for the eight WFC broadband filters, while the smooth curve is a cubic fit to these eight points. If the suspiciously low data for GD153 are eliminated, the fit would shift upward by ∼0.5%. This systematic uncertainty dominates any statistical uncertainties.

Filter	Pivot-WL	%/year	mag/year	2009.6
F220W	2257	0.64	0.0070	...
F250W	2714	0.46	0.0050	...
F330W	3362	0.32	0.0035	...
F344N	3433	0.31	0.0034	...
F435W	4316	0.26	0.0028	1.001
F475W	4761	0.26	0.0028	0.996
F502N	5022	0.26	0.0028	0.995
F550M	5581	0.26	0.0029	0.993
F555W	5358	0.26	0.0029	0.994
F606W	5897	0.26	0.0028	0.994
F625W	6298	0.25	0.0027	0.995
F658N	6583	0.23	0.0025	0.996
F660N	6590	0.23	0.0025	0.996
F775W	7687	0.13	0.0014	1.003
F814W	8091	0.09	0.0009	1.006
F850L	9131	0.	0.	1.011
F892N	8914	0.01	0.0001	1.010

Table 1: *Rate of sensitivity loss in percent per year and in mag per year for each CCD filter. The units of the pivot wavelength column are Angstroms. For the post-SM4 WFC observations, the final column specifies the sensitivities relative to 2002.2 per the curve in Figure 3.*

loss rates. The photometry for GD153 obtained in 2009 is consistently lower than the 2011 points for GD71 and G191B2B for all eight filters in common; but a detailed examination of the individual images does not reveal any obvious flaw in the 2009 data set. As either instrumental or astrophysical explanations are possible for the low GD153 data points early in the post-repair era, a proper definition of the post-2009 sensitivity trends must await the gathering of more data. The adopted constant sensitivities for each WFC filter are the average of the WD observations that are available after SM4, as illustrated in the Figure 1 example for F555W. These average levels after 2009.6 appear in Figure 3, where each value represents the sensitivity relative to the initial sensitivity of unity at 2002.2. The cubic fit in Figure 3 has coefficients 1.218, -9.978e-05, 1.419e-08, and -6.297e-13 as a function of wavelength in Angstroms, while the final column of Table 1 has the evaluations of this cubic at the pivot wavelengths.

The corrections in Table 1 specify the changes to the $photflam, P_\lambda$, flux calibration values in the ACS data headers, i.e. P_λ^o represents the header values for HRC, the original values for WFC at -77C, or the updated values after 2006.5, when the WFC set-point temperature was lowered to -81C.

$$P_\lambda = P_\lambda^o \ (1 + C_3 \ [t - 2002.2]/100), \tag{1}$$

where C_3 is the %/year loss rate from column 3 of Table 1 for 2002–2007 and t is the observation date in decimal years. After 2009,

$$P_\lambda = P_\lambda^o \ C_5, \tag{2}$$

where C_5 is the value from column 5 of Table 1 for post-SM4. For scientific analyses that do not require P_λ values, equivalent corrections can be made to the ACS images or to the extracted photometry. These corrections will not be implemented in the pipeline until confirmed by the on-going investigations of sensitivity changes derived from repeated observations of starfields. After a correction is incorporated into the pipeline calculations of $photflam$, Equations 1–2 should not be applied. If a new QE curve for post-SM4 is implemented or enough time has elapsed to reveal any post-SM4 trends, then Equation 2 should not be used.

3. Analysis of the 47 Tuc Data

Over the ACS lifetime, the same field located five arcmin west of the core of the globular cluster 47 Tuc has been observed many times with HRC and WFC in F435W and all longer wavelength bands. These data are used to define the low-frequency spatial components of the flat fields (Mack et al. 2002), to measure the geometric distortion (Anderson 2007), and to determine CTE losses (Chiaberge 2009, Anderson & Bedin 2010). Using the technique of (Mack et al. 2007) to average over the field, these data could also define the changes in sensitivity; and an analysis might confirm the above results for the WD standards. As an initial check, the WFC observations of 47 Tuc in F606W are examined here.

The photometry for each image is extracted from the $*flt.fits$ images with aperture photometry measured in 3, 5, and 10 pixel radii using the FORTRAN codes from Anderson & King (2006). This photometry is corrected for CTE losses in the observed image with the method of AB10 or in the extracted photometry with the MC09 algorithm; and the measured stellar positions are matched to produce a master catalog. Much of the 10 pixel radius photometry is contaminated due to the crowding in the densely populated 47 Tuc field illustrated in Figure 4. Small sub-regions of this field are shown in Fig. 2 of MC09 and

in Fig. 1 of Mack et al. (2007). However, there are typically ∼1000 bright isolated stars that are used to define aperture corrections for the 3 and 5 pixel radius photometry relative to the 10 pixel (0″.5) reference aperture, as illustrated in Mack et al. (2007). These average aperture corrections for each 47 Tuc image are applied to the 3 and 5 pixel results to produce a final catalog of 143 images in the WFC F606W filter. The repeatability of the three pixel photometry tends to be worse than for the five pixel results, probably because of residual effects of breathing on the HST PSF. Thus, the 5 pixel data are used for our analysis.

For the five pixel data, the F606W photometry of each star in each image is compared to the mean photometry of 18 early 22.5s images that establish an initial baseline obtained on 2002 May 8–9, just after installation of ACS into HST. The peak-to-peak scatter among the 18 baseline images is ±0.3%. These photometric differences are averaged for each image as illustrated in Figure 5 for a typical example. After sigma clipping the red points, the flux-weighted average of the remaining green points is computed. These mean differences using the AB10 CTE correction appear in Figure 6 as a function of time with red for short exposures and blue for long exposure to check for any dependence on exposure time. The two separate fits are shown along with the WD result (green line) of a loss rate of 0.0028 mag/year from §2. Exposure time ranges are 30–140s, and >339s for the short, and long exposures, respectively. Figure 7 displays the same results, except with the MC09 CTE correction. There are ∼4000 measured stars in each short exposure and ∼8000 in the long exposures. The slopes of the various linear fits are in Table 2.

Method	Slope	Loss at 2007.0
WD	0.0028	0.013
AB10 Short	0.0022	0.011
AB10 Long	0.0007	0.003
MC09 Short	0.0009	0.004
MC09 Long	0.0007	0.003

Table 2: *Various results for the slope of the fit to the sensitivity loss in mag per year and total loss in mag after 4.8 years at 2007.0 for F606W, assuming no loss at 2002.2. The different methods used are the WD standard star results from §2, CTE corrections according to AB10, and CTE corrections according to MC09. Results for both the short and long exposures are included for AB10 and MC09 methodologies.*

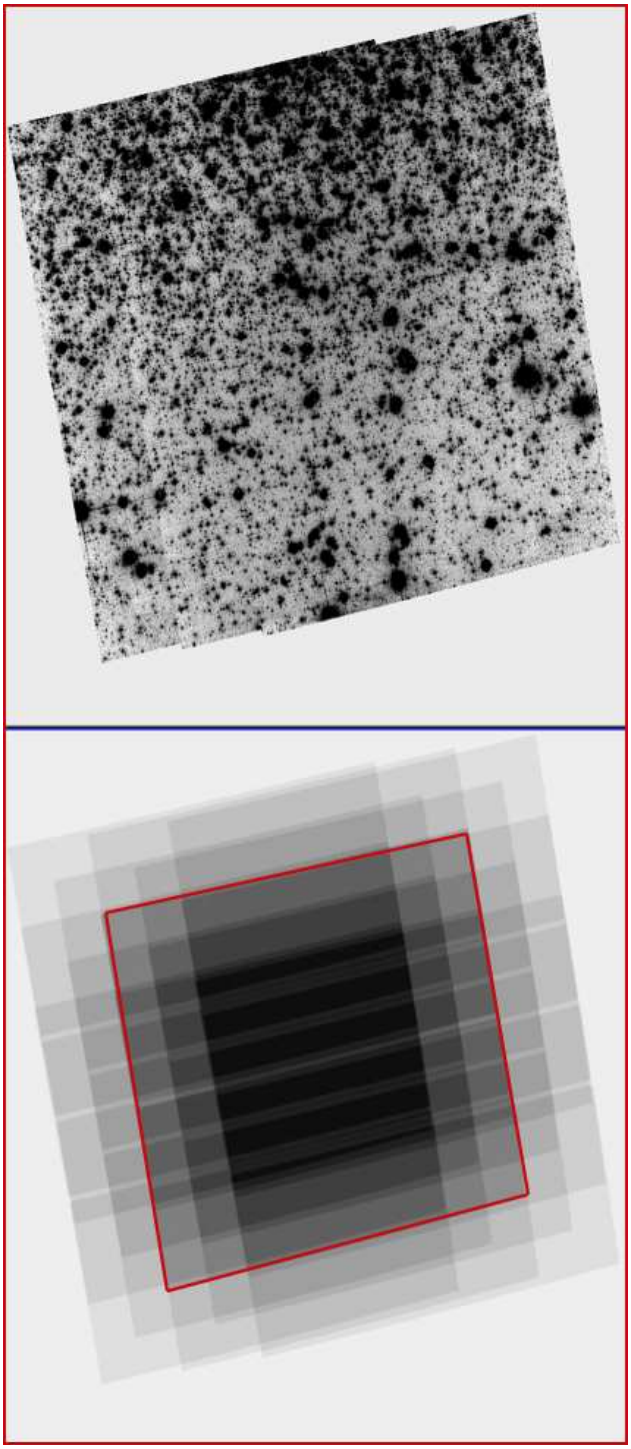

Fig. 4.— (Top:) A drizzled mosaic of the 47 Tuc calibration field observed in F606W following SM4. (Bottom:) The weight image, which is equivalent to an effective exposure time map, for the 14 dither positions, each of which is a 339s exposure. The red box shows the WFC field of view in a single exposure.

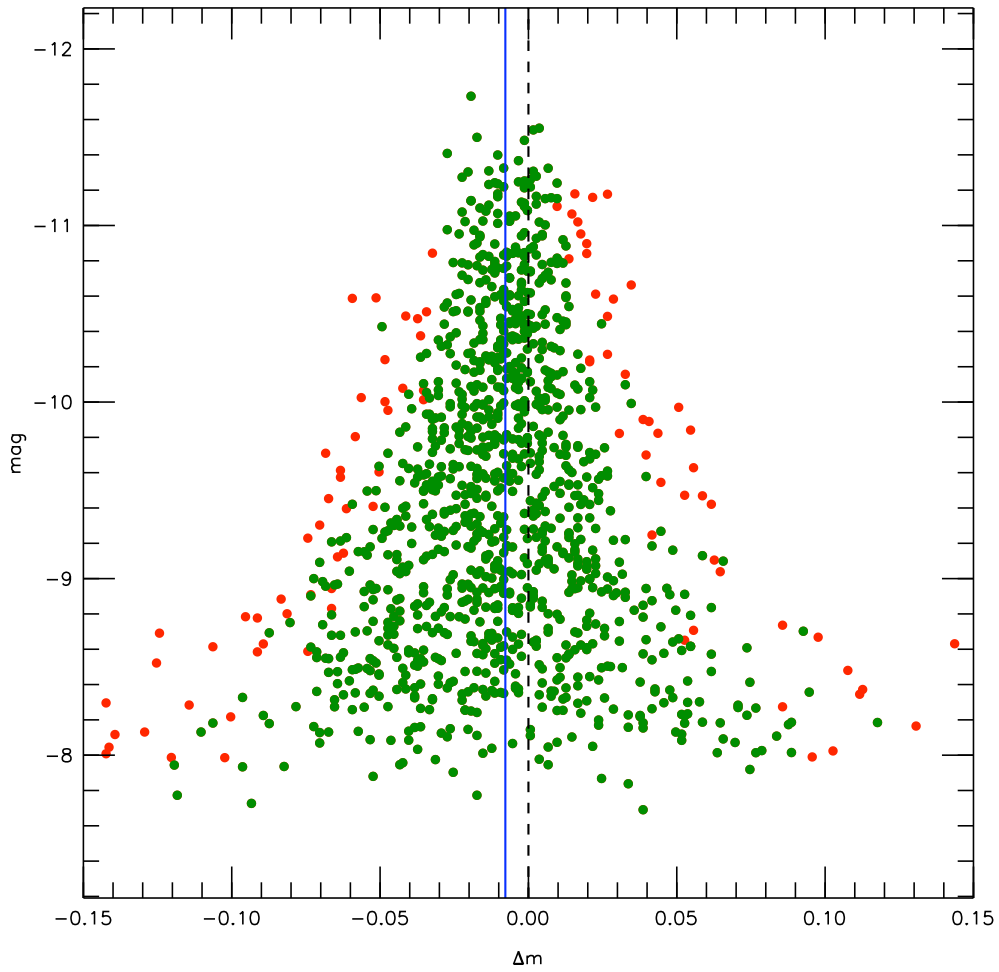

Fig. 5.— Five-pixel photometry for each star in the 30s image $jbbf01i3q\_flt.fits$ of 47 Tuc obtained in 2009 as a function of the differences between $jbbf01i3q$ and a mean of 18 images obtained in 2002. The mag values are in instrumental units, i.e. $-2.5log(electrons)$. The red points are rejected after iterative sigma-clipping and are not included in the weighted average of the remaining 1087 green points. The vertical solid blue line lies at this mean value of -0.0078, which is uncertain by 0.0006.

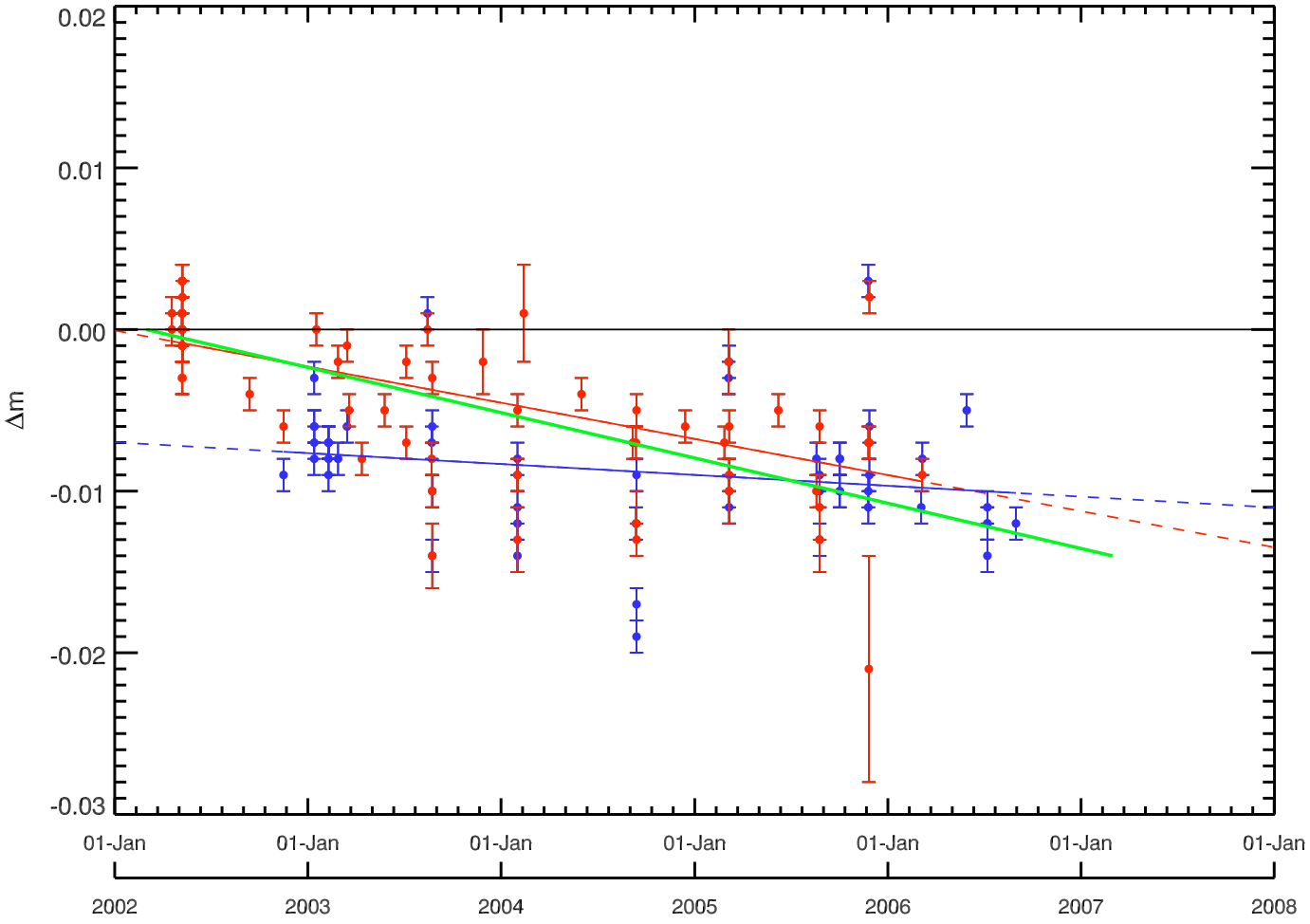

Fig. 6.— The F606W photometry for 47 Tuc relative to a 2002 epoch as a function of time with the CTE corrections as specified by AB10. Each F606W image is averaged as in Figure 5 to produce one data point with error bars. Short exposures are in red, while blue is for long exposures. The green line is the result from Table 1 above and is close to the red line fit for the short exposure set.

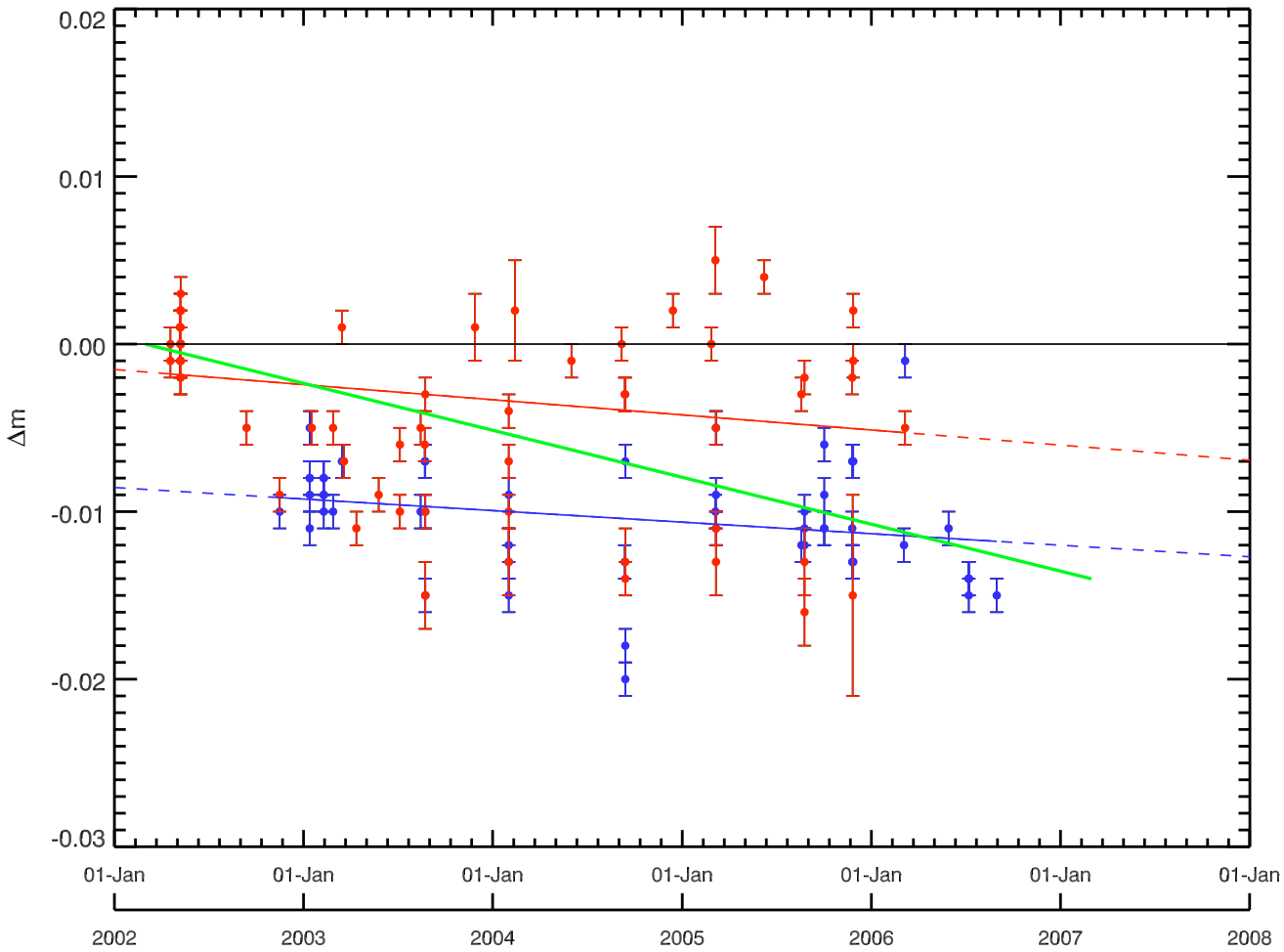

Fig. 7.— As in Figure 6, except for the CTE correction algorithm of MC09. Both fits are flatter than the green line, even though the blue points near 2006 agree fairly well with the green line from the WD results.

4. Discussion

In general, the 47 Tuc loss rates for F606W in Table 2 are less than the WD standard star value of 0.0028 mag/yr. The discrepancy between the AB10 results for the short and long exposures suggests that the uncertainties in the 47 Tuc analysis are too large to confirm the WD results. The AB10 correction were derived using post-SM4 long exposure darks; and more recent studies of the CTE before 2007 show that adjustments are required to the CTE corrections used to make Figure 6. After these updates to the AB10 code to account for the different release rates of the trapped charge at the higher operating temperature in 2002–2006, Figure 6 should be reconstructed.

For the MC09 results shown in Figure 7, the long exposures have a similar slope but show an offset from the shorter set, which is evidence for a problem with the sky subtraction in the crowded 47 Tuc field (cf. Dolphin 2000). Whether there is a systematic error in the sky estimates or whether the apparent discrepancy is just a deficiency in the non-linear CTE correction requires more study. One approximation in the Figure 7 is that the MC09 CTE correction is for three pixel radius photometry, while those three-pixel coefficients are applied to our five pixel results. MC09 tested their three-pixel corrections on five-pixel photometry with good success at the 0.1 mag level but did not present results at the sub-0.01 mag level required for measuring the time dependent sensitivity losses of 0.003 mag/year. The largest systematic deviations of the 47 Tuc data from the green WD line in Figure 7 are only $\sim$0.005 mag for the clump of blue points near 2003. Another approximation lies in the functional form assumed by MC09, i.e. the local sky level to a negative power, which is undefined for the zero or slightly negative sky levels found in short exposures. A more physical formulation for the STIS CTE uses an exponential of the negative ratio of sky to stellar signal (Bohlin & Goudfrooij 2003, Goudfrooij et al. 2006). In crowded fields, there is often a nearby star in the readout direction that fills the charge traps; and a better approximation would be to use a larger range sky average that includes some signal from the neighboring stars. The best quantitative estimates of the uncertainty in the MC09 CTE corrections are provided in their table 2, which lists the three CTE correction coeficients and the three corresponding formal uncertainties. Applying the MC09 CTE correction to the 47 Tuc data with coefficients in the quoted range of uncertainty can produce a loss rate that agrees with the 0.003 mag/year WD result.

In conclusion, neither the AB10 or MC09 CTE correction techniques currently have adequate precision to robustly reveal the small sensitivity losses derived from the WD analysis. However, refinements to the techniques, especially for AB10, are under study and may produce corrections to the large 47 Tuc dataset that are precise enough to confirm or improve the loss rates implied by the observations of the bright WD standards. If a long vs.

short exposure discrepancy is still apparent after applying improved CTE corrections, then an improved method of extracting the photometry must be developed before the 47 Tuc dataset can be used to determine reliable loss rates for the ACS CCD cameras.

References

Anderson, J. 2007, Instrument Science Report, ACS 2007-08, (Baltimore:STScI)

Anderson, J., & King, I. R. 2006, Instrument Science Report, ACS 2006-01, (Baltimore:STScI)

Anderson, J., & Bedin, L. R. 2010, PASP, **122**, 1035 (AB10)

Bohlin, R. C. 2007, Instrument Science Report, ACS 2007-06, (Baltimore:STScI) (B07)

Bohlin, R. C., & Anderson, J. 2011, Instrument Science Report, ACS 2011-01, (Baltimore:STScI)

Bohlin, R. C. 2011, Instrument Science Report, ACS 2011-02, (Baltimore:STScI)

Bohlin, R. C., & Goudfrooij, P. 2003, Instrument Science Report, STIS 2003-03R, (Baltimore:STScI)

Bohlin, R. C., et al. 2011, AJ, 141, 173

Chiaberge, M., et al. 2009, Instrument Science Report, ACS 2009-01, (Baltimore:STScI) (MC09)

De Marchi, G., Sirianni, M., Gilliland, R., Bohlin, R., Pavlovsky, C., Jee, M., Mack, J., van der Marel, R., & Boffi, F. 2004, Instrument Science Report, ACS 2004-08, (Baltimore:STScI)

Dolphin, A. E. 2000, PASP, 112, 1397

Gilliland, R. L., Bohlin, R. C., & Mack, J. 2006, Instrument Science Report, ACS 2006-06, (Baltimore:STScI)

Goudfrooij, P., Bohlin, R. C., Maiz-Apellaniz, J., & Kimble, R. 2006, PASP, 118, 1455

Grogin, N., Lim, P. L., Maybhate, A., Hook, R., & Loose, M. 2010, 2010 HST Calibration Workshop, S. Deustua & C. Oliveira, eds., (Baltimore:STScI)

Mack, J., Bohlin, R., Gilliland, R., Van der Marel, R., Blakeslee, J., & DeMarchi, G. 2002, Instrument Science Report, ACS 02-08, (Baltimore:STScI)

Mack, J., Gilliland, R. L., Anderson, J., & Sirianni, M. 2007, Instrument Science Report, ACS 2007-02, (Baltimore:STScI)

Sirianni, M., et al. 2005, PASP, 117, 1049S (S05)

Sirianni, M., Gilliland, R., & Sembach, K. 2006, Technical Instrument Report, ACS TIR 2006-02, (Baltimore:STScI)

Stys, D. J., Bohlin, R. C. & Goudfrooij, P. 2004, Instrument Science Report, STIS 2004-04, (Baltimore:STScI)